A conceptual hydraulic conductivity model for unsaturated soils at low degree of saturation and application to the study of capillary barrier systems

by Riccardo Scarfone[1*], Simon J. Wheeler[2*] & Marti Lloret-Cabot[3]

Abstract: Accurate modelling and prediction of the variation of hydraulic conductivity of unsaturated soils at very low degree of saturation has important implications in various engineering problems. Physical processes underlying the hydraulic behaviour of unsaturated soils (retention behaviour and variation of hydraulic conductivity) are firstly explained and then a consistent set of new definitions for key transition hydraulic states is proposed. This lays the foundation for the presentation of a new predictive hydraulic conductivity model, accurate for the full range of degree of saturation and applicable to relatively coarse-grained soils (i.e. gravels, sands and silts). The hydraulic conductivity is divided into two components: a bulk water component and a liquid film component; each of which varies with degree of saturation or suction. The model is then validated against experimental data. Finally, the new hydraulic conductivity model is applied to the numerical study of the hydraulic behaviour of capillary barrier systems (CBSs). The new model is able to predict the behaviour of CBSs better than conventional models and the numerical modelling highlights the role of liquid film flow, which is often neglected.

1. Introduction

The hydraulic properties of unsaturated soils are described by the soil water retention curve (SWRC), namely the relationship between degree of liquid saturation S_l and suction s, and the soil hydraulic conductivity curve (SHCC), namely the relationship between hydraulic conductivity k and either degree of saturation or suction. Many hydraulic constitutive models describing mathematically the SWRC and the SHCC have been proposed. Conventionally, water retention models are empirical and their parameter values for a given soil are typically calibrated with experimental data. On the other hand, models for the SHCC generally rely on information from

[1]M.Sc., Ph.D. candidate, Marie Sklodowska-Curie Early Stage Researcher, Riccardo.scarfone@glasgow.ac.uk, School of Engineering, University of Glasgow, Rankine Building, Oakfield Avenue, Glasgow G128LT, UK. ***Corresponding author**.

[2]Ph.D., Cormack Professor of Civil Engineering, Simon.Wheeler@glasgow.ac.uk, School of Engineering, University of Glasgow, Rankine Building, Oakfield Avenue, Glasgow G128LT, UK. ***Corresponding author**.

[3]Ph.D., Assistant Professor, marti.lloret-cabot@durham.ac.uk, Department of Engineering, Durham University, South Road, Durham DH1 3LE, UK.

the SWRC model, typically with the saturated hydraulic conductivity k_s as the only additional parameter value required to fully define the SHCC. Direct experimental measurements of unsaturated hydraulic conductivity over the full range of degree of saturation or suction are relatively rare (and normally limited to the research field), because they are time-consuming, technically complex and expensive.

The conventional water retention models proposed by Brooks and Corey (1964), van Genuchten (1980) and Kosugi (1996) are amongst the most well-known. All three of these empirical models for the SWRC can generally provide a good match to the SWRC at high and moderate values of degree of saturation, but they cannot accurately represent the SWRC at low values of S_l. All three models predict that S_l tends asymptotically to a minimum value, termed the "residual degree of saturation" S_{lr}, as suction tends to infinity. However, experimental results (Campbell and Shiozawa 1992), supported by thermodynamic considerations (Richards 1965), show that the value of S_l reduces to zero at a finite value of suction of approximately 1 GPa. Hence, some more recently proposed SWRC models are specifically intended to extend the range of application to lower degree of saturation. Some of these models involve new mathematical expressions (Fredlund and Xing 1994) whereas others are modified forms of previous conventional models (Campbell and Shiozawa 1992; Rossi and Nimmo 1994; Fayer and Simmons 1995; Zhang 2011; Khlosi *et al*. 2006; Peters 2013; Iden and Durner 2014; Peters 2014).

Similar to the water retention models, many conventional models for the SHCC provide realistic modelling of the variation of hydraulic conductivity at medium and high values of the degree of saturation but they do not perform well at low values of degree of saturation. Among these, Brooks and Corey (1964) proposed a semi-empirical model for the prediction of the SHCC, utilizing the similitude between the character of the SWRC and the SHCC. Burdine (1953) and Mualem (1976b) proposed statistical models making use of the fact that the unsaturated hydraulic conductivity depends on the pore-size distribution. They modelled the soil pores as a bundle of cylindrical tubes, with each individual tube either filled or empty of water with the liquid flow attributed to the former. However, these models are inappropriate at low values of degree of saturation where few if any pores are entirely filled with water and these do not form continuous liquid paths. In these conditions, the liquid flow occurs only within thin liquid films covering the surfaces of the soil particles and in meniscus water bridges at the inter-particle contacts. More recently, SHCC models incorporating the role of liquid films have been developed. Although these models have been shown to represent well the SHCC at very low degree of saturation (as well as at moderate and high values of S_l), most of them are mathematically complex (Tuller

and Or 2001), not predictive (Peters and Durner 2008; Peters 2013) or involve parameter values that must be determined from experimental data that are difficult to obtain with sufficient accuracy (Lebeau and Konrad 2010).

Accurate representation of the hydraulic properties of unsaturated soils at low degree of saturation is particularly important for coarse-grained soils, which tend to desaturate easily (i.e. at low values of suction). The thickness of liquid films, which decreases with increasing suction, is higher at low values of suction and hence higher water fluxes occur within the liquid films. When very fine soils (e.g. clays) desaturate, i.e. at very high values of suction, the liquid films are so thin that the molecular attractions inhibit liquid movement within the liquid films (Kemper 1961). Thus, a model for the SHCC able to represent accurately the behaviour of unsaturated soils over the full range of S_l, but which also remains predictive and simple to apply, is proposed in this paper for relatively coarse-grained soils (i.e. gravels, sands and silts).

Modelling the hydraulic behaviour of unsaturated soils at low values of degree of saturation is important in a variety of applications. One of these is the modelling of the hydraulic behaviour of the coarser layer of a capillary barrier system (Scarfone *et al*. 2018), which is typically at very low degree of saturation. Capillary barrier systems (CBSs) are geotechnical structures made of a finer-grained layer (F.L.) overlying a coarser-grained layer (C.L.), placed over the original soil with the aim of reducing or limiting the percolation of rainwater into the underlying ground (Stormont and Anderson 1999). Under typical operating conditions, the coarser layer is at very low degree of saturation (much lower values of S_l than the finer layer). As a consequence, in contrast to saturated conditions, the coarser layer will typically be much less hydraulically conductive than the finer layer. Hence, prior to significant water breakthrough into the coarser layer, the coarser layer acts as an almost impermeable barrier, whereas the infiltrating rainwater is stored in the overlying finer layer. However, as increasing amounts of infiltrating rainwater are stored in the finer layer, the suction at the interface between the two layers decreases. If this suction at the interface decreases sufficiently, the coarser layer becomes conductive and breakthrough of water from the finer layer into the coarser layer occurs, making the CBS fail.

The failure of the barrier (i.e. the breakthrough phenomenon) has been studied extensively (Baker and Hillel 1990; Stormont and Anderson 1999; Yang *et al*. 2004; Yang *et al*. 2006). Breakthrough occurs when the liquid phase filling the pores first forms continuous liquid paths across the interface between the finer layer and the coarser layer. This occurs when the suction at the interface attains the breakthrough value of the coarser layer,

corresponding to the point at which the hydraulic conductivity of the coarser layer increases dramatically. Experimental studies also showed that no significant water movement is observed across the interface before breakthrough and, when breakthrough occurs, it is always a relatively sudden phenomenon compared to the overall period of rainfall infiltration. When the infiltration rate is very low, the water breakthrough from the finer layer to the coarser layer may occur in the form of fingering instead of a homogeneous advancing wetting front (Baker and Hillel 1990). In the interest of simplicity, the phenomenon of fingering is not considered in this work, but it is thought to only influence post-breakthrough behaviour, rather than the conditions when breakthrough occurs.

In this paper, an overview of the hydraulic behaviour of unsaturated soils is initially given and some key transition points on the SWRC and on the SHCC are identified and defined. This serves as the physical basis for the development of a new hydraulic constitutive model, which is presented and validated against experimental data. This new hydraulic constitutive model is intended for relatively coarse-grained soils (i.e. gravels, sands and silts). The impact of this new model is then assessed in the numerical study of the hydraulic behaviour of a CBS, carried out by means of the CODE_BRIGHT finite element software (Olivella *et al*. 1996).

2. Hydraulic behaviour of unsaturated soils

The definition and explanation of liquid-gas arrangement states at key transition points is often unclear and inconsistent in the literature. For instance, the "residual degree of saturation" is defined in different ways by different authors (Vanapalli *et al*. 1998): the horizontal asymptote of the SWRC (Brooks and Corey 1964), the degree of saturation at s=1500 kPa (van Genuchten 1980), the degree of saturation corresponding to the maximum amount of water in a soil not contributing to liquid flow (Luckner *et al*. 1989) or simply a fitting parameter (van Genuchten 1980; Kosugi 1996; Luckner *et al*. 1989). Similar lack of clarity applies to the definition of the "water-entry" value (Hillel and Baker 1988; Bouwer 1966). Therefore, it is important to give a consistent and clear explanation and definition of the different liquid-gas arrangement states at key transition points on the SWRC and SHCC, as a basis for subsequent development of hydraulic constitutive models.

An unsaturated soil is made of three phases: the liquid phase, the gas phase and the solid phase. Liquid pore water is divided into three forms: bulk water, meniscus water and liquid film water (see Fig. 1). Bulk water is the water occupying those void spaces that are completely flooded, whereas meniscus water is the water bridges which surround the inter-particle contact points that are not covered by bulk water (Wheeler and

110 Karube 1996). Liquid film water consists of thin liquid films covering the surfaces of the soil particles when
111 pores are filled with air. Liquid films surrounding different soil particles are connected by means of the
112 meniscus water bridges at the inter-particle contacts. The presence of liquid film water is governed by
113 adsorptive forces (Israelachvili 2011), mainly ionic-electrostatic and molecular, and its contribution is often
114 neglected during modelling of water retention and hydraulic conductivity. In contrast to clays, where liquid
115 films occur only at high values of suction and the films are then so thin that they are tightly bound to the
116 surfaces of soil particles, liquid films can occur at relatively low values of suction in coarser-grained soils and
117 the films are then sufficiently thick that they behave as free water in terms of mobility. Therefore, advective
118 liquid flow occurs within adsorbed liquid films in relatively coarse-grained soils (Kemper 1961; Tuller and Or
119 2001; Lebeau and Konrad 2010).

120 The SWRC of a soil is directly related to the liquid-gas distribution states. Fig. 2a shows a typical main
121 wetting curve and a typical main drying curve in a semi-logarithmic plot. These two curves differ because the
122 water retention behaviour of unsaturated soils is typically hysteretic (Haines 1930). Fig. 2a shows also the
123 relationship between SWRCs and pore-water forms in unsaturated soils and some key transition points on the
124 SWRCs are highlighted. As shown in Fig. 2a, different gas-liquid distribution states can be identified,
125 depending on the degree of saturation: they are defined as capillary state, funicular state and pendular state
126 (Schubert *et al*. 1975). In the capillary state, at low suction, the soil is saturated ($S_l = 1$), all the pores are filled
127 with liquid water and only bulk water is present. For intermediate values of degree of saturation and suction,
128 in the funicular state, gas and liquid phases coexist. In this case, liquid water is present in the forms of bulk
129 water, meniscus water bridges and liquid films. For low degree of saturation and high suction, the soil is in the
130 pendular state, all the pores contain air, there is no bulk water left and liquid water is present only in the forms
131 of meniscus water bridges and liquid films.

132 Following a drying path starting from a saturated state (see the main drying curve shown in Fig. 2a), the
133 soil is in the capillary state until suction is increased up to the air-entry value (AE). At this point, air starts
134 entering the voids, firstly into the voids with the largest entry throats, and the soil enters the funicular state. As
135 the suction increases from the air-entry value, air breaks through into more voids, with smaller and smaller
136 entry throats. The degree of saturation gradually falls, mainly because the volume of bulk water decreases but
137 also because, although the number of meniscus water bridges and the area of particle surfaces covered by liquid
138 films both increase as new pores fill with air, the volume of each individual meniscus water bridge decreases

with increasing suction (Fisher 1926) and the thickness of the liquid films also decreases with increasing suction (Tokunaga 2009). When the degree of saturation reduces to the air-continuity value (AC), the gas phase starts forming continuous gas paths within the soil. At the bulk-water discontinuity point (BWD), although bulk water is still present in the soil, it occupies so few voids that the bulk water no longer forms continuous liquid paths. Decreasing the degree of saturation further, the bulk water-exclusion point (BWEX) represents the filling of the last voids with air, so that there is no longer any bulk water, and this corresponds to the transition from the funicular state to the pendular state. From this point onwards, a large increase in suction corresponds to a small decrease in degree of saturation, due only to the reduction in size of meniscus water bridges and reduction in thickness of liquid films. Ultimately, the soil completely dries for a suction value s_{dry} of approximately 1 GPa (Richards 1965; Campbell and Shiozawa 1992). Lu and Khorshidi (2015) used a water vapor sorption-based method to show that the value of s_{dry} ranges between about 0.5 GPa and 1 GPa for different soils.

Similar concepts apply to a wetting path starting from a dry state (see the main wetting curve shown in Fig. 2a). At the bulk water-entry point (BWE), bulk water starts filling the smallest voids, representing a transition from the pendular state to the funicular state. At the bulk water-continuity point (BWC), sufficient voids are filled with bulk water to form a continuous liquid path, whereas at the air-discontinuity point (AD) the gas phase becomes discontinuous. Eventually, at the air-exclusion point (AEX), air is totally removed and the soil enters the capillary state. When a main wetting SWRC is obtained experimentally, air can remain trapped in the soil and complete saturation may not be reached even when zero suction is imposed on the external boundary of the soil sample. In this case, the wetting SWRC appears to be approximately horizontal from the point AD where the gas phase becomes discontinuous, as shown by the dashed line in Fig. 2a. However, this dashed line does not represent true equilibrium states, because the trapped air is at elevated pressure (i.e. the internal value of suction within the soil sample is greater than the value applied at the boundary) and the trapped air is then expelled very slowly by the processes of air dissolution and diffusion in the liquid phase.

Points AE, AEX, BWEX and BWE are directly related to the shape of the SWRC. AE and AEX can be identified as the points where the main drying curve and main wetting curve respectively diverge from a fully saturated condition (S_l=1). Since the degree of saturation has been shown to decrease approximately linearly with the logarithm of suction in the pendular state (i.e. no bulk water) (Campbell and Shiozawa 1992), BWEX and BWE can be identified as the points where the two curves (in the semi-logarithmic plot) diverge from an

approximately linear relationship at low degree of saturation (see Fig. 2a). In contrast, the points AC, AD, BWD and BWC are not related to the shape of the SWRC. BWD and BWC are related to the shape of the SHCC (see Fig. 2b), as they represent transitions between states where bulk water flow occurs (in which case this completely dominates the hydraulic conductivity) and states where liquid water flow occurs only through liquid films. AC and AD are only important in the variation of gas conductivity, with the gas conductivity as zero for suction values lower than these points.

In the literature, there is often no distinction between the bulk water-exclusion point BWEX, bulk water-entry point BWE, bulk water-continuity point BWC and bulk water-discontinuity point BWD (see Fig. 2). They are all often defined as the "residual" point, which is typically identified as the bend in the SWRC at low degree of saturation, when plotted in semi-logarithmic form (Vanapalli *et al*. 1998; Tami *et al*. 2004; Zhan and Ng 2004).

Liquid water flow in unsaturated soils may occur within continuous liquid paths formed by the bulk water and/or by the thin liquid films, connected to each other at the inter-particle contacts by means of meniscus water bridges. Thus, the hydraulic conductivity k of unsaturated soils can be split in two components: the bulk water component k^{Bulk} and the liquid film component k^{Film}. The film flow component is ignored in many SHCC models, which assume that liquid water flows only through pores filled with bulk water. This assumption is reasonable for very fine soils (e.g. clays) because, in these soils, flow through voids filled with bulk water completely dominates liquid flow up to very high values of suction (e.g. >10 MPa for a clay) and at these very high values of suction, the thickness of the adsorbed liquid films, which decreases with increasing suction, is so small (e.g. <1 nm) that the attractive molecular forces between water molecules and the surfaces of the soil particles impede any mobility of the water within the liquid films. However, for coarser soils (e.g. sands), the contribution of adsorbed liquid films to liquid flow becomes dominant at much lower values of suction than in fine-grained soils (e.g. 10 kPa), and at these values of suction the thickness of the films may be orders of magnitude higher (e.g. >20 nm). In this case, the molecular attractions, strong only in the first molecular layers next to the soil particle surfaces, do not impede the liquid film flow (Kemper 1961; Tuller and Or 2001; Lebeau and Konrad 2010). Whereas the role of adsorbed liquid films in contributing to hydraulic conductivity is more important for coarser-grained soils than for clays, the contribution of liquid films to water retention behaviour and mechanical behaviour is most important in clays (Lu and Likos 2006).

196 The value of hydraulic conductivity depends on the number and the size of the continuous liquid paths
197 formed by the water. In particular, the more and larger are these liquid paths, the higher is the hydraulic
198 conductivity. Fig. 2b shows typical main drying and main wetting SHCCs in a log-log plot. The difference
199 between these two curves is mainly due to the water retention hysteresis, because the hydraulic conductivity
200 variation generally shows very little hysteresis when k is plotted against S_l. In the capillary state, the soil is
201 saturated ($S_l = 1$) and thus, the hydraulic conductivity is equal to the saturated value k_s. In this condition, k^{Film}
202 $= 0$ and $k = k^{Bulk} = k_s$. In the funicular state, as suction increases, k^{Bulk} reduces from the saturated value, because
203 the continuous flow channels formed by bulk water are fewer and fewer and restricted to the smaller channels
204 and voids. Moreover, the lengths of the continuous flow channels also increase because the tortuosity of these
205 paths increases. Although k^{Film} is greater than zero in this condition, it is negligible if compared to k^{Bulk} in
206 almost all the funicular range. In the pendular state, no bulk water is present within the soil. More precisely, it
207 is at the bulk water-discontinuity point BWD during drying that k^{Bulk} falls to zero or at the bulk water-continuity
208 point BWC during wetting that k^{Bulk} starts increasing from zero (see Fig. 2b), because at these points the liquid
209 paths formed by the bulk water become respectively discontinuous or continuous. For suctions above the bulk
210 water-discontinuity point (during drying) or the bulk water-continuity point (during wetting), the hydraulic
211 conductivity is very small (several orders of magnitude smaller than the saturated value) and related only to
212 the liquid paths formed by the thin liquid films connected by meniscus water bridges at the inter-particle
213 contacts, so that $k^{Bulk} = 0$ and $k = k^{Film}$. Moreover, as suction increases, the hydraulic conductivity $k = k^{Film}$
214 decreases (see Fig. 2b), because the thickness of liquid films and the size of liquid bridges both decrease with
215 increasing suction.

216 **3. New hydraulic constitutive model**

217 This Section presents a SWRC model and a SHCC model that are both suitable for use in relatively coarse-
218 grained soils (gravels, sands and silts) over the full range of degree of saturation. The SWRC model is an
219 existing (but non-conventional) model proposed by Fayer and Simmons (1995), whereas the SHCC model is
220 new. The performances of these models are qualitatively compared with those of the conventional van
221 Genuchten (1980) SWRC model and Mualem (1976b) SHCC model.

222 3.1 SWRC

223 The van Genuchten (1980) (VG) model is one of the most widely used SWRC models. It relates the effective
224 degree of saturation S_{le} to the suction s:

$$S_{le} = \left[1 + (\alpha s)^n\right]^{-m} \quad (1)$$

where α, n and m are parameters of the model (soil constants). Parameters m and n are often correlated as m=1-1/n (van Genuchten 1980). The degree of saturation S_l is then calculated as:

$$S_l = S_{lr} + (S_{ls} - S_{lr}) \cdot S_{le} \quad (2)$$

where S_{lr} and S_{ls} are two further constants, representing the residual degree of saturation and the maximum degree of saturation (at s=0) respectively. According to Eqs. 1 and 2, the residual degree of saturation S_{lr} is the value of S_l as s tends to infinity. More typically, however, it is simply treated as a fitting parameter of the VG model, to optimise the fit to the experimental variation of S_l in the funicular range. In this paper, the term residual degree of saturation is only used to refer to this fitting parameter, used exclusively in the conventional van Genuchten model. The maximum degree of saturation S_{ls} appearing in Eq. 2 is typically assumed as S_{ls} = 1, to represent achievement of saturated conditions at s =0.

As stated earlier, the van Genuchten model is not accurate at low values of degree of saturation. Therefore, an alternative SWRC model, the modified van Genuchten (modVG) model proposed by Fayer and Simmons (1995), is used in this study. In the modVG model, the variation of degree of saturation is still given by Eqs. 2 and 1, but S_{lr} is no longer a constant and instead S_{lr} varies with suction according to:

$$S_{lr} = \xi \ln\left(\frac{s_{dry}}{s}\right) \quad (3)$$

where s_{dry} is the suction at which S_l goes to zero and ξ is a fitting parameter, obtained by fitting the model to SWRC data at low degrees of saturation. The parameter s_{dry} is typically assumed as s_{dry} = 1 GPa.

A comparison between the performance of the VG model and the modVG model is shown in Fig. 3a, where the two models are employed to fit experimental data over the full range of S_l. The experimental data set is for Shonai sand (Mehta *et al*. 1994) and will be discussed in more detail in Section 3.3 (soil 6). The SWRCs obtained with the VG model and the modVG model are almost coincident in the capillary and funicular states, where both models fit the experimental data well. However, the modVG model is able to represent effectively also the pendular state, where the degree of saturation decreases approximately linearly with the logarithm of suction down to a completely dry state (Campbell and Shiozawa 1992).

3.2 SHCC

The Mualem (1976b) (M) model is commonly used to describe the SHCC, in particular when it is coupled with the van Genuchten (1980) model for the SWRC. In the Mualem model, the soil is assumed as a homogeneous porous medium with a certain statistical pore size distribution, which is indirectly related to the shape of the SWRC. The water is assumed to flow only in bulk water-filled pores which are modelled as bundles of cylindrical capillary tubes of different radii. If the Mualem model is coupled with the van Genuchten SWRC model, the hydraulic conductivity k is given by:

$$k = k_s \sqrt{S_{le}} \left[1 - \left(1 - S_{le}^{1/m} \right)^m \right]^2 \tag{4}$$

where k_s is the saturated hydraulic conductivity. This means that, once the SWRC is defined by the VG model, only one extra parameter is needed (i.e. k_s) for the description of the SHCC by the M model.

The accuracy of the Mualem model, when coupled with the van Genuchten model, deteriorates as the degree of saturation decreases, failing completely when the degree of saturation is so low that the bulk water is discontinuous. The model has two main weaknesses. Firstly, the model is not able to represent the liquid flow occurring in the liquid films and in the meniscus water bridges at very low values of degree of saturation. Secondly, applying Eq. 1 (the VG SWRC model) in Eq. 4 (the M SHCC model), the hydraulic conductivity goes to zero only when suction tends to infinity. This is physically unreasonable if this model is used only to represent the bulk water component of the hydraulic conductivity, as k^{Bulk} must, in reality, go to zero at the BWD point during drying and diverge from zero at the BWC point during wetting.

Due to these shortcomings of the conventional M model, a new hydraulic conductivity model, that is more accurate than the M model at low degree of saturation, is now proposed. In the new model, the hydraulic conductivity k is considered as the sum of two terms, as proposed by (Peters 2013):

$$k = k^{Bulk} + k^{Film} \tag{5}$$

The bulk water component of the SHCC k^{Bulk} is modelled with an expression similar to the M model (Eq. 4) but the variable S_{le} occurring twice in Eq. 4 is replaced by two different variables. The term $\sqrt{S_{le}}$ occurring in the right hand-side of Eq. 4 was introduced by Mulalem (1976b) to model the increase of tortuosity and decrease of connectivity between bulk water-filled pores with decreasing degree of saturation. According to Eq. 1, S_{le} goes to zero only when suction goes to infinity, which produces unreasonable results in Eq. 4. In reality, the connectivity of the bulk water is lost for suction values equal to or higher than the BWD point (drying) or the BWC point (wetting). Thus, a new term $\sqrt{S_l^C}$ is used instead of $\sqrt{S_{le}}$, where S_l^C is defined by:

$$S_l^C = \frac{S_l - S_{l,BWD}}{1 - S_{l,BWD}} \quad \text{for drying} \qquad S_l^C = \frac{S_l - S_{l,BWC}}{1 - S_{l,BWC}} \quad \text{for wetting} \tag{6}$$

where $S_{l,BWD}$ and $S_{l,BWC}$ are the values of degree of saturation at the BWD point and at the BWC point respectively. The second appearance of S_{le} in the right hand-side of Eq. 4 was introduced by Mualem (1976b) to model the decrease of the number and size of pores filled with bulk water with decreasing degree of saturation. Again, using S_{le} from Eq. 1 is unreasonable, because this implies that the quantity of bulk water goes to zero only when suction goes to infinity. In reality, the volume of the bulk water is zero for suction values equal to or higher than the BWEX point (drying) or the BWE point (wetting). Thus, a new variable S_l^B is used instead:

$$S_l^B = \frac{S_l - S_{l,BWEX}}{1 - S_{l,BWEX}} \quad \text{for drying} \qquad S_l^B = \frac{S_l - S_{l,BWE}}{1 - S_{l,BWE}} \quad \text{for wetting} \tag{7}$$

where $S_{l,BWEX}$ and $S_{l,BWE}$ are the values of the degree of saturation at the BWEX and BWE points respectively. Thus, the bulk water component of the relative hydraulic conductivity can be expressed with a new modified version of the Mualem model (modM model), as follows:

$$k^{Bulk} = k_s \sqrt{S_l^C} \left[1 - \left(1 - \left(S_l^B \right)^{1/m} \right)^m \right]^2 \tag{8}$$

The values of $S_{l,BWD}$, $S_{l,BWC}$, $S_{l,BWEX}$ and $S_{l,BWE}$ (for use in Eqs. 6 and 7) may be difficult to identify experimentally. Akin and Likos (2017) identified the BWE point (which they defined as the adsorption-capillary transition point) as the change in slope of water sorption isotherms (i.e. curves of water content plotted against relative humidity obtained under isothermal conditions). Identification of the values of $S_{l,BWD}$ and $S_{l,BWC}$ may be particularly challenging, given that these values should strictly be determined from high quality experimental SHCC data at low values of S_l and this type of data is rarely available. However, in the absence of more precise data, a simplified pragmatic procedure can be used, which assumes $S_{l,BWD} = S_{l,BWEX}$ and $S_{l,BWC} = S_{l,BWE}$. This simplified graphical procedure, which uses only the SWRC, is similar to that suggested by Vanapalli *et al*. (1999) and is illustrated in Fig. 4. With the fitted SWRC (based on the modVG model of Eqs. 1-3) presented in a semi-logarithmic plot, the intersection point of the tangent through the inflection point of the main drying curve and the straight line formed by the final linear portion of the main drying curve defines a suction $s_{BWD/BWEX}$ (see Fig. 4). The value of $S_{l,BWD} = S_{l,BWEX}$ is then taken as the value of S_l on the fitted main drying curve at the suction $s_{BWD/BWEX}$ (see Fig. 4). A corresponding procedure using the main wetting curve

gives the value of $S_{l,BWC} = S_{l,BWE}$ (see Fig. 4). Assuming $S_{l,BWD} = S_{l,BWEX}$ means that $S_l^C = S_l^B$ during drying and, similarly, assuming $S_{l,BWC} = S_{l,BWE}$ means that $S_l^C = S_l^B$ during wetting (see Eqs. 6 and 7). This simplified procedure is likely to underestimate the values of $S_{l,BWD}$ and $S_{l,BWC}$ and overestimate the values of $S_{l,BWEX}$ and $S_{l,BWE}$ (see Fig. 2), resulting in overestimation of S_l^C and underestimation of S_l^B. These errors will therefore partially compensate when Eq. 8 is used to determine the value of k^{Bulk}.

In order to model the liquid film component of the hydraulic conductivity k^{Film}, a predictive semi-empirical model is proposed (LF model). In the pendular state, where the flow occurs only within the liquid films, the relationship between hydraulic conductivity and suction has been shown to be approximately linear in the log-log plot, with a slope of approximately -1.5 (Tokunaga 2009; Lebeau and Konrad 2010; Zhang 2011; Peters 2013). This slope of -1.5 has a theoretical basis from Tokunaga (2009), who derived an analytical expression for the liquid flow occurring within liquid films in an idealized soil consisting of identically-sized smooth spherical particles, for the situation where none of the voids are filled with bulk water and hence all of the particles are covered by liquid films. The slope of -1.5 was subsequently validated against experimental data from different types of natural soils, including sands, loams and a sandy clay (Lebeau and Konrad 2010; Zhang 2011; Peters 2013). This would suggest the following relationship within the pendular range:

$$k^{Film} = C^{Film} \cdot s^{-1.5} \tag{9}$$

where C^{Film} is a model parameter (soil constant). Eq. 9 would represent the liquid film component of the hydraulic conductivity if there was no bulk water over the full range of s. However, increasing amounts of liquid film are replaced by bulk water in the funicular range and hence k^{Film} should drop to zero at full saturation, whereas Eq. 9 gives k^{Film} tending to infinity as s tends to zero. In practice, accurate modelling of k^{Film} is unnecessary within the funicular and capillary states, because liquid flow in these states is completely dominated by bulk water flow. A pragmatic approach is therefore proposed, which involves the introduction of a dummy parameter a:

$$k^{Film} = C^{Film} \cdot \left(a + s\right)^{-1.5} \tag{10}$$

The effect of the dummy parameter a should be negligible in the range of suction where liquid films govern the liquid flow (Tokunaga, 2009). The value of a must be small enough that it does not affect the linearity of the log-log plot at very low values of S_l (in the pendular range), but large enough that the predicted value of

k^{Film} is negligible compared to k^{Bulk} at high values of S_l. Using a value of the parameter a between $s_{BWD}/100$ and $s_{BWD}/10$ for drying and between $s_{BWC}/100$ and $s_{BWC}/10$ for wetting is typically acceptable.

If high quality experimental SHCC data at low values of S_l are available for the particular soil, these can be used to determine the value of the soil constant C^{Film} in Eq. 10. However, such data are rarely available, because the hydraulic conductivity in this range is very low and thus not easy to measure. In the absence of such data, the value of C^{Film} can be estimated from knowledge of a representative particle size of the soil and of the porosity ϕ. Tokunaga (2009) showed analytically that, for a soil made of identical spherical particles of diameter D, the value of k^{Film} at a given value of s varies linearly with $(1-\phi)/D$. Hence, the following relationship is proposed for the estimation of the parameter C^{Film}:

$$C^{Film} = X_D \frac{1-\phi}{D} \tag{11}$$

where D is a representative particle size for the soil and X_D is a model parameter (a soil constant). The effective particle size D_{10} is suggested for the parameter D, because liquid film flow is likely to be predominantly controlled by the size of the smaller soil particles (because of their high specific surface area). This was confirmed by finding a better statistical correlation of experimental data from different soils when using D_{10}, rather than when using D_{50} or D_{90} (see Section 3.3). However, values of D_{10} are not always available (e.g. when the fines content is high and hence D_{10} is very small) and, in this case, the value of D_{50} can be used instead. The parameter X_D accounts for factors not appearing in Eq. 11, such as differences in particle shapes, particle-size distribution and soil fabric between different soils. However, the value of X_D is expected to vary over a limited range for different coarse-grained soils, and hence, in the absence of data to determine a soil-specific value for X_D, a default value, applicable to all coarse-grained soils, can be assumed. The choice of this default value for X_D will depend upon whether D_{10} or D_{50} is used for D in Eq. 11, as described below in Section 3.3.

A comparison between the hydraulic conductivity models presented above is shown in Fig. 3b, with the models used to predict the bulk water component of the hydraulic conductivity of the Shonai sand (Mehta *et al*. 1994) (see soil 6 in Section 3.3) and to fit the liquid film component. Fig. 3b is plotted in terms of relative hydraulic conductivity k_r, defined as $k_r=k/k_s$. At high values of S_l, the conventional M model and the new modM+LF model lead to very similar SHCCs but, as S_l decreases, greater differences arise between the two models. In particular, around the BWC point the conventional M model overestimates the hydraulic conductivity (by about two orders of magnitude for the Shonai sand), whereas the new modM+LF model

predicts much lower values of k, because k^{Bulk} goes to zero at the BWC point. The overestimation of k in this region by the conventional M model is most evident for coarse-grained soils (Reinson *et al*. 2005). In contrast, at high values of suction the conventional M model underestimates the hydraulic conductivity, because it does not take into account the role of liquid film flow. Finally, it can be seen that in the new modM+LF model the hydraulic conductivity is governed almost entirely by k^{Bulk} at relatively low suction values and almost entirely by k^{Film} at relatively high suction values. The predicted transition between the two, occurring around the BWC point, is sharper and more distinct for coarser soils.

Fig. 5 shows a qualitative comparison between the predicted SHCCs from the new SHCC model for two soils: a coarser-grained soil and a finer-grained soil. The coarser soil has a higher saturated hydraulic conductivity but transitions between capillary, funicular and pendular states occur at lower values of suction than in the finer soil and, thus, the liquid film component of the hydraulic conductivity becomes dominant at a lower value of suction. Comparing the two soils in the suction range where the hydraulic conductivity is governed by the liquid film component, it can be seen that, at the same value of suction (points A_f and A_c in Fig. 5), the hydraulic conductivity is higher for the finer soil. At the same value of suction, the thickness of the adsorbed liquid films is the same for the two soils but the finer soil has a higher specific surface area and thus a higher number of liquid film flow channels. This effect is represented by the dependence of C^{Film} on representative particle size D in Eq. 11. However, at the two different suction values where the liquid film component of the hydraulic conductivity becomes dominant over the bulk water component for the two soils (points B_f and B_c in Fig. 5), the hydraulic conductivity of the coarser soil is higher than that of the finer soil, because the thickness of the adsorbed liquid films is much greater at point B_c than at point B_f. This explains why considering the contribution of liquid film flow to hydraulic conductivity is more relevant for coarser-grained soils than for finer-grained soils.

At extremely high suction values, approaching s_{dry}, the liquid film flow becomes so small that water movement will be dominated by vapor flow (i.e. diffusion of water within the gas phase) (Peters, 2013). However, unlike the advective liquid water flux, which is governed by Darcy's law, the diffusive flux of water vapor within the gas phase is a different physical process, governed by Fick's law. Thus, flow of water vapor cannot be included in the hydraulic conductivity k. Some numerical codes, including CODE_BRIGHT, include both vapor diffusion, modelled by Fick's law, and advective liquid flux, modelled by Darcy's law. In this way, the two different phenomena of advective liquid water flux and diffusive water vapor flux are both correctly

389 modelled. The distinction is particularly important when coupled thermo-hydraulic problems are analysed. It
390 is worth mentioning that experimental measurements of k at very low values of S_l must always be treated with
391 caution because it can be difficult to distinguish water movements due to liquid flow and water movements
392 due to vapor flow, unless experiments are specifically designed with this purpose.

393 It is possible that water movements due to liquid flow and water movements due to vapor flow are not
394 entirely separate physical processes at a continuum scale (i.e. at a scale significantly larger than individual soil
395 particles or voids) once the bulk water is discontinuous, because water might move by series/parallel flow in
396 the form of vapour through gas-filled voids and in the form of liquid water across meniscus water bridges, as
397 described by Philip and de Vries (1957) (vapour condensing on one side of each meniscus water bridge and
398 evaporating on the other side of the meniscus water bridge). This mechanism is relevant for non-isothermal
399 flows being driven by temperature gradients. The model presented in this paper cannot account for this type
400 of combined liquid/vapour flow, with transfers between liquid and vapour phases occurring repeatedly at a
401 length scale of the order of the void size. Consideration of this phenomenon would lead to a greater amount of
402 water vapour flow than that predicted considering liquid water flow and water vapour flow as separate
403 phenomena, with an increase typically lower than one order of magnitude (Philip and de Vries 1957; Cass *et*
404 *al*. 1984). This aspect may be relevant for high temperature gradients and at high values of suction where water
405 movement within liquid films is comparable or lower than water movement due to vapour transfer but it is
406 likely to be negligible at relatively low values of suction, just above s_{BWC} or s_{BWD}, where water movement
407 within liquid films is several orders of magnitude greater than water movement due to vapour transfer.

408 It should be noted that the proposed new hydraulic constitutive model has a small element of inconsistency,
409 in that the modVG SWRC model predicts that the value of S_l reduces to zero (i.e. no liquid water present in
410 the soil) at a finite (but extremely high) value of suction s_{dry}, whereas the proposed modM+LF SHCC model
411 predicts that the hydraulic conductivity only goes to zero as suction tends to infinity. For most practical
412 problems this inconsistency has negligible effects because, at very high suction values approaching s_{dry}, water
413 movement is dominated by vapor diffusion.

414 3.3 Experimental validation of the model

415 Data from tests on 11 relatively coarse-grained soil samples were used for experimental validation of the
416 new hydraulic model. Properties of these soils (soil type, reference, saturated hydraulic conductivity k_s and
417 porosity) are shown in Table 1. The experimental data come from three different sources: a journal paper

(Mehta *et al*. 1994), the unsaturated soil hydraulic database UNSODA (Nemes *et al*. 2001) and an unsaturated soil hydraulic catalogue (Mualem 1976a). Experimental data defining the SWRC and the SHCC were available for all 11 soils. For soil 8, unlike the other soils, the SHCC data points were only available in the k:S_l plot, but they were converted to the k:s plot by using the modVG model for the SWRC. This operation was considered reasonable, because the modVG model was able to fit the experimental SWRC points extremely well over the full range of suction for this soil.

Experimental SHCC data in the suction range where hydraulic conductivity was governed by the liquid film component (low values of S_l) were available for soils 1-10. For these soils, the expression for k^{Film} given by Eq. 10 (LF model) was fitted to the experimental SHCC data points in the suction range where these points could be approximated by a straight line with slope -1.5 in the log-log scale, as shown in Fig. 6 (which is plotted in terms of relative hydraulic conductivity k_r). In this fitting operation, the slope of the straight line in the log-log plot was fixed *a priori* to -1.5 whereas the parameter C^{Film} was fitted. In all 10 soils, the LF model fits the experimental data very well. This confirms the validity of Eq. 10, including the value of the exponent (-1.5). The resulting values of the parameter C^{Film} are shown in Table 2. The units employed for C^{Film} in Table 2 are appropriate if suction s and parameter a are expressed in kPa and k^{Film} is required in units of m/s.

Among soils 1-10, values of D_{10} were available for soils 1-6 and values of D_{50} were available for soils 1-8 (see Table 1). For each of these soils, the fitted value of C^{Film} shown in Table 2 was combined with the soil porosity ϕ and the appropriate value of D_{10} or D_{50} to back-calculate a corresponding soil-specific value of the parameter X_D (see Table 2), by using Eq. 11. The units employed for X_D in Table 2 are appropriate if suction s and parameter a are expressed in kPa, representative particle size D (i.e. D_{10} or D_{50}) is expressed in mm and k^{Film} is required in units of m/s. When using D_{10}, the geometric mean of the 6 soil-specific values of X_D listed in Table 2 was calculated as 2.35×10^{-9} $mm.ms^{-1}.kPa^{1.5}$ (see Table 2), and this is recommended as a general default value of X_D to use in Eq. 11 (with a value of D_{10}) in cases where experimental values of k in the pendular range (low values of S_l) are not available. If a value for D_{10} is not available, but D_{50} is known, the corresponding default value of X_D is 1.08×10^{-8} $mm.ms^{-1}.kPa^{1.5}$ (see Table 2). However, it is preferable to use D_{10}, if possible, because statistical analysis showed that the variance in the D_{10} soil-specific values of X_D shown in Table 2 is less than the variance in the D_{50} soil-specific values of X_D. The statistical analysis of the D_{10} soil-specific values of X_D indicated a 95% confidence level that the value of X_D for a soil should fall between a lower bound of 0.2 times the default value and an upper bound of 5 times the default value.

Experimental and modelled SWRCs and SHCCs for all the 11 soils are shown in Fig. 7, with the SHCCs plotted in terms of relative hydraulic conductivity k_r. In the graphs representing the SWRCs, the experimental points are compared to the conventional VG model and the proposed modVG model, both fitted to the experimental SWRC points. In both cases, the constraint m=1-1/n was used and the parameter S_{ls} was set as S_{ls}=1. Values of the remaining model parameters are shown in Table 3. In the graphs representing the SHCCs, the experimental points are compared to the conventional M model (coupled with the VG model) and the new modM+LF model (coupled with the modVG model for the prediction of k^{Bulk}). In the k^{Bulk} component (i.e. modM) of the new SHCC model, the value of the parameter $s_{BWD} = s_{BWEX}$ for each soil (see Table 3), and hence the value of $S_{l,BWD} = S_{l,BWEX}$, was obtained from the SWRC using the graphical construction described in Section 3.2 (see Fig. 4). In the k^{Film} (i.e. LF) component of the new SHCC model, the value of C^{Film} was taken either as a fitted value, from Table 2, where SHCC data from the pendular range were available (soils 1-10), or as a predicted value, calculated from Eq. 11, using the appropriate default value of X_D (see Table 2) and the value of D_{10}, where this was available (soils 1-6, 11), or the value of D_{50} (soils 7, 8).

For soils where SWRC data were available in the pendular range (i.e. soils 3, 6, 9 and 10), the modVG model fits the experimental data much better than the VG model (see Fig. 7). However, in the capillary and funicular ranges, the two models are indistinguishable.

Fig. 7 also shows that in general the modM model predicts k^{Bulk} better than the M model. Exceptions are soil 3 where the two models lead to very similar results and soils 1 and 2 where both models are not in a good agreement with the experimental data. This mis-match for soils 1 and 2 is probably related to an underlying weakness of the Mualem approach or to inaccurate experimental determination of the value of k_s (note that the experimental values of k within the funicular range have not been used at all in determining the parameter values in the modM+LF model). The difference between the M model and the modM model may lead to significant differences of hydraulic conductivity for certain values of suction. For instance, at the BWD point of soil 10 (s=8 kPa), the conventional M model overestimates the hydraulic conductivity by approximately three orders of magnitude.

Fig. 7 shows that the liquid film branch of the SHCCs for the different soils is very well modelled by Eq. 10 when this is fitted to experimental data (i.e. using a fitted value of C^{Film}). Moreover, it can be seen that, in the absence of experimental data of hydraulic conductivity at very low degree of saturation, k^{Film} may be predicted adequately by Eqs. 10 and 11, if an appropriate default value of X_D, presented in Table 2, is used.

For soil 11, experimental SHCC points were not available at very low degree of saturation and the liquid film component of the SHCC model could only be predicted. This is an example of how the predictive SHCC model should be used in the absence of experimental data.

4. Numerical application to the study of capillary barrier systems

The new hydraulic constitutive models for unsaturated soils (modVG for SWRC and modM+LF for SHCC) were implemented in the CODE_BRIGHT finite element code (Olivella *et al*. 1994, 1996). Numerical simulations of one-dimensional infiltration tests on a capillary barrier were then performed with the new hydraulic constitutive models and with the conventional (VG-M) models. The aims of these analyses were: i) to show that the new improved hydraulic models are able to describe better the properties of the breakthrough condition from the finer layer to the coarser layer and ii) to assess the role of liquid films in the behaviour of CBSs. Only isothermal liquid transport was considered in the analyses, with the solid phase considered as non-deformable and the gas phase as non-mobile. Thus, constant and uniform values of temperature (T = 20 °C), displacements of the solid phase (u = 0m) and gas pressure (u_a = 0kPa) were imposed. The influence of vapor diffusion within the gas phase was investigated by performing two versions of each simulation: the first with vapor diffusion not considered and the second with vapor diffusion included.

4.1 Material and methods

The numerical model was a vertical column of soil made of two layers: an upper layer, 0.5m thick, representing the finer layer (F.L.) of a CBS and a lower layer, 0.75m thick, representing the coarser layer (C.L.) (see Fig. 8a). The thickness of the coarser layer was unrealistically high in order to have the bottom boundary sufficiently far from the interface so that the phenomenon of breakthrough was not affected by any influence of the bottom boundary. The materials forming the two layers were each modelled by defining the hydraulic constitutive models (SWRC and SHCC) and the porosity. Each of the two layers was considered as a uniform material. The parameters chosen to model the finer layer were representative of a silty sand whereas those of the coarser layer were representative of a pea gravel. The finer layer was modelled using the conventional van Genuchten-Mualem (VG-M) model because, in the analyses, this layer was never at very low degree of saturation. The coarser layer was modelled using the following combinations of models: i) van Genuchten-Mualem (VG-M); ii) modified van Genuchten-modified Mualem (modVG-modM); and iii) modified van Genuchten-modified Mualem + liquid film (modVG-modM+LF). For the modVG-modM+LF modelling, the value of X_D was taken as the default value of 2.35 x 10^{-9} mm.ms^{-1}.kPa$^{1.5}$ in all the analyses presented here, but

some further simulations were performed using X_D values 5 times larger and 5 times smaller, to explore the impact of uncertainty in the value of this parameter. The parameter values of the materials are shown in Table 4 and the SWRCs and SHCCs are shown in Fig. 8b and Fig. 8c respectively.

The initial condition for the numerical analyses was a hydrostatic pore-water pressure profile, with u_w = 0 kPa (s = 0 kPa) at the bottom boundary, u_w = -12.5 kPa (s = 12.5 kPa) at the top, and a linear variation between. In this initial condition, the coarser layer was at very low degree of saturation (lower than $S_{l,BWC}$).

For the bottom boundary condition, a constant value of the pore-water pressure equal to the initial value was imposed, namely u_w= 0 kPa. For the top boundary condition, a constant value of vertical water flux (the infiltration rate) was imposed. In order to assess the influence of the infiltration rate, two values of water flux were considered: $i_1 = 10^{-6}$ m/s and $i_2 = 10^{-8}$ m/s. The value of i_1 was chosen so that it was comparable with the saturated hydraulic conductivity of the finer layer ($3x10^{-6}$ m/s) whereas i_2 was two orders of magnitude smaller than i_1 and representative of a low rainfall intensity.

4.2 Results and discussion

The results of the numerical analyses of the infiltration process in a CBS are presented here in order to highlight the influence of the SHCC models used for the coarser layer and the influence of the liquid film conductivity, which is commonly neglected.

In this set of analyses, the fitted value of S_{lr} of the coarser layer in the VG model is close to 0 and therefore the VG and modVG models lead to very similar SWRCs (see Fig. 8b). Hence, the choice between them does not significantly affect the results of the analyses in this case and all the differences which are shown below are attributable to the use of different SHCCs, rather than to the use of different SWRCs. The results shown in Figs. 9 and 10 are for the simulations with vapor diffusion excluded, but vapor diffusion was found to have negligible effect in most cases, as discussed later.

Fig. 9 shows the predicted time histories of the effective vertical velocity of the liquid phase (flow rate per unit plan area) predicted at the interface between the finer and coarser layers, obtained using different infiltration rates and different hydraulic constitutive models for the coarser layer. In all the simulations, the effective water velocity at the interface is initially equal to zero. A wetting front then starts moving downwards from the ground surface until it reaches the interface (located at 0.5m below the top boundary). The suction at the interface then decreases and some time later water starts moving across the interface (breakthrough). The

533 estimated times at breakthrough are indicated by symbols in Fig. 9. Soon after breakthrough, the water velocity
534 across the interface becomes equal to the infiltration rate applied at the surface (see Fig. 9).

535 It can be seen from Fig. 9 that the predicted breakthrough takes different forms, depending on the infiltration
536 rate and on the model used to describe the hydraulic behaviour of the coarser layer. At the lower infiltration
537 rate i_2, the use of the conventional VG-M model to describe the behaviour of the coarser layer results in
538 prediction that breakthrough would be a relatively gradual phenomenon. In contrast, when the new modVG-
539 modM or modVG-modM+LF models are used for the coarser layer, the numerical simulations show
540 breakthrough as a relatively sudden phenomenon at both infiltration rates. These predictions with the new
541 models are a better qualitative match to experimental observations (Stormont and Anderson 1999), which show
542 that breakthrough is always a very sudden phenomenon, irrespective of the infiltration rate. Inspection of Fig.
543 9 also shows that, particularly at the lower infiltration rate i_2, use of the conventional VG-M model results in
544 prediction of an earlier time to breakthrough than is predicted by the new modVG-modM or modVG-
545 modM+LF models. This means that the conventional VG-M model predicts a lower water storage capacity of
546 the finer layer prior to breakthrough than the new models.

547 The analysis of the suction profile at breakthrough is very important in the study of a CBS because it allows
548 the water content profile at breakthrough to be obtained by means of the SWRC, and this allows the water
549 storage capacity of the barrier to be calculated, where the water storage capacity is defined as the maximum
550 amount of water that can be stored in the barrier before breakthrough occurs (Stormont and Morris 1998).
551 According to experimental observations, starting from initial conditions when the barrier is generally at low
552 water contents (relatively high suction values), the rainwater infiltrating from the surface causes changes in
553 the suction profile in the finer layer. The infiltrating rainwater is initially stored entirely within the finer layer,
554 which causes the water content to increase and the suction to decrease. When the suction at the interface
555 approaches the BWC value of the coarser layer, this becomes hydraulically conductive and water breaks
556 through from the finer layer to the coarser layer.

557 Figs. 10a and 10b show the suction profiles at the time of breakthrough predicted by the numerical analyses
558 for infiltration rates i_1 and i_2 respectively. Also shown, for comparison, are the initial suction profile and a
559 simple empirical suction profile in the finer layer at the time of breakthrough. The latter was obtained by
560 imposing the BWC value of the coarser layer (0.7 kPa) at the interface and above this a hydrostatic profile up
561 to a limiting suction value corresponding to the suction at which the hydraulic conductivity of the finer layer

562 is equal to the applied infiltration rate (this limiting suction is reached only in the case of the higher infiltration
563 rate i_1). Various authors (e.g. Stormont and Morris 1998) observed experimentally that the suction profile in
564 the finer layer at the time of breakthrough was always very close to this empirical approximation. From Figs.
565 10a and 10b, it can be seen that the use of the conventional VG-M model leads to results that are different to
566 the experimental observations from the literature and, again, these differences are more significant for low
567 infiltration rates. In particular, with the VG-M model, breakthrough is predicted when the suction value at the
568 interface is higher than the BWC suction value of the coarser layer and, furthermore, this predicted suction
569 value at the interface varies with the infiltration rate (whereas experimental observations indicate that the
570 suction value at the interface at the time of breakthrough is independent of infiltration rate). By contrast, these
571 inconsistencies with experimental observations are not seen if the new modVG-modM or modVG-modM+LF
572 models are used for the coarser layer. The numerical results for the suction profile in the finer layer at the time
573 of breakthrough (see Figs. 10a and 10b) are then almost identical to the simplified empirical suction profile at
574 breakthrough, which was reported to be a good approximation of experimental observations. Using the
575 modVG-modM model, breakthrough is predicted to occur when the suction at the interface exactly reaches the
576 BWC value of the coarser layer, when bulk water starts forming continuous liquid networks across the
577 interface. In addition, the liquid film flow, included in the modVG-modM+LF model, does not affect the
578 suction profiles in the finer layer at the time of breakthrough (see Figs. 10a and 10b).

579 The liquid film component of the SHCC may, however, affect significantly the suction profile in the coarser
580 layer at the time of breakthrough. Using the modVG-modM model, the predicted suction profile in the coarser
581 layer at the time of breakthrough is identical to the initial suction profile (see Figs. 10a and 10b), because only
582 bulk water flow is included in the model and this does not start across the interface until the time of
583 breakthrough. By contrast, when the modVG-modM+LF model, which includes the liquid film flow, is used,
584 the predicted suction profile in the coarser layer at the time of breakthrough is substantially different to the
585 initial suction profile, particularly at the lower infiltration rate (see Fig. 10b), because even before breakthrough
586 of bulk water occurs, a small amount of water flows across the interface through the continuous liquid film
587 networks. This causes a very small increase in the degree of saturation in the coarser layer immediately below
588 the interface (almost insignificant, as shown in the degree of saturation profiles in Figs. 10c and 10d) but a
589 large decrease in suction (Figs. 10a and 10b). This is explained by the shape of the SWRC at low degree of
590 saturation (below $S_{l,BWE}$), where a small increase of S_l corresponds to a large decrease in suction. The predicted

591 changes in the suction profile in the coarser layer prior to breakthrough may have important consequences
592 when CBSs are used for suction control purposes (e.g. Rahardjo *et al*. 2012).

593 The values of S_l predicted in the finer layer with the VG-M model are smaller than those predicted by the
594 new models (see Figs. 10c and 10d). This can be explained by the fact that, with the VG-M model,
595 breakthrough occurred earlier and at higher suction values.

596 Additional simulations were performed to investigate the sensitivity of results to the choice of value for the
597 parameter X_D, which controls the film flow in the coarser layer if the value of C^{Film} is determined from Eq. 11.
598 These additional simulations used values of X_D that were 5 times larger and 5 times smaller than the default
599 value listed in Table 4 (see Fig. 8), covering the 95% confidence interval described in Section 3.3. The results
600 indicated that, within this range, the value of X_D had little influence on the predicted time history of water
601 velocity at the interface (including the phenomenon of breakthrough) or the predicted suction profile in the
602 finer layer at the time of breakthrough. The value of X_D did however affect significantly the predicted suction
603 profile in the coarser layer at the time of breakthrough for the lower infiltration rate i_2. This was expected,
604 because of the previous conclusion that, at the lower infiltration rate, film flow significantly affects the
605 predicted suction profile in the coarser layer at the time of breakthrough (compare the modVG-modM and
606 modVG-modM+LF curves in Fig. 10b). Although the suction profile at the time of breakthrough was
607 significantly affected by the value of X_D, the corresponding degree of saturation profile was only slightly
608 affected.

609 As mentioned before, the role of vapor diffusion was investigated by performing two versions of each
610 numerical simulation, with vapor diffusion either included or excluded. Vapour diffusion had no noticeable
611 effect in the simulations where the coarser layer was represented by either the conventional VG-M model or
612 the new modVG-modM+LF model. In both these cases, although only small amounts of liquid water flow into
613 the coarser layer occurred prior to breakthrough, even these small liquid water flows were much greater than
614 the water flows due to vapor diffusion (Peters 2013). The effect of vapor diffusion had a small but noticeable
615 effect on the results of the simulations employing the modVG-modM model (particularly for the low
616 infiltration rate). With this modVG-modM model, the value of k^{Bulk} reduces to zero at the BWC point and there
617 is no liquid film flow. This means that, with this model, vapor diffusion was the only possible mechanism for
618 water flow into the coarser layer prior to breakthrough. Although the simulations demonstrated that, with the
619 coarser layer represented by either the conventional VG-M model or the new modVG-modM+LF model, vapor

620 diffusion had no noticeable effect on the behaviour of a CBS subjected to a constant rate of infiltration, this
621 does not mean that vapor diffusion will be unimportant in all problems involving unsaturated soils. In
622 particular, water vapor diffusion is likely to be of crucial importance in highly non-isothermal problems, such
623 as nuclear waste disposal (Gens, 2010).

624 **5. Conclusions**

625 Key transition points on the soil water retention curve (SWRC) and soil hydraulic conductivity curve
626 (SHCC) have been identified and defined. This serves as the physical basis for the development of a new
627 predictive hydraulic conductivity model, intended for use over the full range of degree of liquid saturation S_l,
628 particularly for relatively coarse-grained soils (gravels, sands and silts). The new hydraulic conductivity model
629 avoids some inconsistencies in conventional hydraulic conductivity models (e.g. the van Genuchten-Mualem
630 model) which are apparent at low values of S_l.

631 In the new model, the hydraulic conductivity is split into two components: the bulk water component and
632 the liquid film component. The bulk water component is represented by a new modified version of the Mualem
633 model, able to capture the fact that bulk water flow ceases when the bulk water network becomes
634 discontinuous. As in the conventional Mualem model, the bulk water component of hydraulic conductivity in
635 the new model can be predicted simply from knowledge of the saturated hydraulic conductivity k_s and
636 information about the SWRC. The liquid film component of hydraulic conductivity is represented by a semi-
637 empirical relationship. This relationship involves a soil constant that can either be evaluated by fitting
638 experimental values of hydraulic conductivity in the low degree of saturation range (where water flow is only
639 in the liquid films) or it can be estimated from the effective particle size D_{10} and the porosity ϕ. This means
640 that, in the absence of experimental measurements of hydraulic conductivity under unsaturated conditions, the
641 new model can be used to predict the SHCC over the full range of S_l based solely on knowledge of the SWRC
642 and the values of k_s, D_{10} and ϕ. The new model has been validated against experimental data.

643 The new hydraulic constitutive model has been implemented in the CODE_BRIGHT finite element
644 software and applied in a numerical study of the hydraulic behaviour of capillary barrier systems. The new
645 model is able to predict the phenomenon of water breakthrough from the finer layer to the coarser layer of a
646 capillary barrier system much better than the conventional van Genuchten-Mualem model. Moreover, the new
647 model is able to capture the role of the liquid film flow, which is often neglected in numerical modelling. The
648 simulations presented in the paper show that the liquid film flow can have a significant influence on the

variation of suction in the coarser layer of a capillary barrier system, even prior to breakthrough, particularly at low infiltration rates.

The new hydraulic constitutive model is expected to find many other applications in situations where liquid flow occurs in coarse-grained soils at very low degree of saturation, such as during evaporation from a ground surface consisting of a coarse-grained soil.

6. Data Availability Statement

Some or all data, models, or code generated or used during the study are available in a repository online in accordance with funder data retention policies. The online repository is the institutional repository "Enlighten" of the University of Glasgow and the data can be accessed using the following DOI: http://dx.doi.org/10.5525/gla.researchdata.1018.

7. Acknowledgments

The authors wish to acknowledge the support of the European Commission via the Marie Skłodowska-Curie Innovative Training Networks (ITN-ETN) project TERRE 'Training Engineers and Researchers to Rethink geotechnical Engineering for a low carbon future' (H2020-MSCA-ITN-2015-675762).

8. References

Akin, I. D., & Likos, W. J. (2017). "Implications of surface hydration and capillary condensation for strength and stiffness of compacted clay." *Journal of Engineering Mechanics*, 143(8), 04017054.

Baker, R. S., and Hillel, D. (1990). "Laboratory tests of a theory of fingering during infiltration into layered soils." *Soil Science Society of America Journal*, 54(1), 20–30.

Bouwer, H. (1966). "Rapid field measurement of air entry value and hydraulic conductivity of soil as significant parameters in flow system analysis." *Water Resources Research*, 2(4), 729–38.

Brooks, R., and Corey, T. (1964). "Hydraulic properties of porous media." *Hydrology Papers*, Colorado State University, 3, 1–27.

Burdine, N. T. (1953). "Relative permeability calculations from pore size distribution data." *Journal of Petroleum Technology*, 5(3), 71–78.

Campbell, G. S., and Shiozawa, S. (1992). "Prediction of hydraulic properties of soils using particle-size distribution and bulk density data." *Indirect methods for estimating the hydraulic properties of unsaturated soils*, 317–28. University of California, Riverside.

677 Cass, A., Campbell, G. S., and Jones, T. L. (1984). "Enhancement of thermal water vapor diffusion in
678 soil." *Soil Science Society of America Journal*, 48(1), 25-32.
679 Fayer, M. J., and Simmons, C. S. (1995). "Modified soil water retention functions for all matric suctions."
680 *Water Resources Research*, 31(5), 1233-1238.
681 Fisher, R. A. (1926). "On the capillary forces in an ideal soil; correction of formulae given by WB
682 Haines". *The Journal of Agricultural Science*, 16(3), 492-505.
683 Fredlund, D. G., and Xing, A. (1994). "Equations for the soil-water characteristic curve." *Canadian*
684 *geotechnical journal*, 31(4), 521-532.
685 Gens, A. (2010). “Soil-environment interactions in geotechnical engineering.” *Géotechnique*, 60(1), 3.
686 Hillel, D., and Baker, R. S. (1988). "A descriptive theory of fingering during infiltration into layered
687 soils." *Soil Science*, 146(1), 51-56.
688 Iden, S. C., and Durner, W. (2014). "Comment on “Simple consistent models for water retention and
689 hydraulic conductivity in the complete moisture range” by A. Peters". *Water Resources Research*, 50(9),
690 7530-7534.
691 Israelachvili, J. N. (2011). *Intermolecular and surface forces (Third Edition)*. San Diego: Academic
692 Press.
693 Kemper, W. D. (1961). "Movement of Water as Effected by Free Energy and Pressure Gradients: I.
694 Application of Classic Equations for Viscous and Diffusive Movements to the Liquid Phase in Finely Porous
695 Media 1." *Soil Science Society of America Journal*, 25(4), 255-260.
696 Khlosi, M., Cornelis, W. M., Gabriels, D., and Sin, G. (2006). "Simple modification to describe the soil
697 water retention curve between saturation and oven dryness." *Water Resources Research*, 42(11).
698 Kosugi, K. I. (1996). "Lognormal distribution model for unsaturated soil hydraulic properties." *Water*
699 *Resources Research*, 32(9), 2697-2703.
700 Lebeau, M., and Konrad, J. M. (2010). "A new capillary and thin film flow model for predicting the
701 hydraulic conductivity of unsaturated porous media." *Water Resources Research*, 46(12).
702 Lu, N., and Khorshidi, M., (2015), "Mechanisms for soil-water retention and hysteresis at high suction
703 range," *Journal of Geotechnical and Geoenvironmental Engineering*, 141(8): 04015032.
704 Lu, N., and Likos, W. J. (2006). "Suction stress characteristic curve for unsaturated soil." *Journal of*
705 *geotechnical and geoenvironmental engineering*, 132(2), 131-142.

706 Luckner, L., van Genuchten, M. T., and Nielsen, D. R. (1989). "A consistent set of parametric models for
707 the two-phase flow of immiscible fluids in the subsurface." *Water Resources Research*, 25(10), 2187-2193.
708 Mehta, B. K., Shiozawa, S. H. O., and Nakano, M. (1994). "Hydraulic properties of a sandy soil at low
709 water contents." *Soil science*, 157(4), 208-214.
710 Mualem, Y. (1976a). “A Catalogue of the Hydraulic Properties of Unsaturated Soils.” Haifa, Israel:
711 Technion Israel Institute of Technology, Technion Research & Development Foundation.
712 Mualem, Y. (1976b). "A new model for predicting the hydraulic conductivity of unsaturated porous
713 media." *Water resources research*, 12(3), 513-522.
714 Nemes, A. D., Schaap, M. G., Leij, F. J., and Wösten, J. H. M. (2001). "Description of the unsaturated
715 soil hydraulic database UNSODA version 2.0." *Journal of Hydrology*, 251(3-4), 151-162.
716 Olivella, S., Carrera, J., Gens, A., and Alonso, E. E. (1994). "Nonisothermal multiphase flow of brine and
717 gas through saline media." *Transport in porous media*, 15(3), 271-293.
718 Olivella, S., Gens, A., Carrera, J., and Alonso, E. E. (1996). "Numerical formulation for a simulator
719 (CODE_BRIGHT) for the coupled analysis of saline media." *Engineering computations*, 13(7), 87-112.
720 Peters, A. (2013). "Simple consistent models for water retention and hydraulic conductivity in the
721 complete moisture range." *Water Resources Research*, 49(10), 6765-6780.
722 Peters, A. (2014). "Reply to comment by S. Iden and W. Durner on “Simple consistent models for water
723 retention and hydraulic conductivity in the complete moisture range”." *Water Resources Research*, 50(9),
724 7535-7539.
725 Peters, A., and Durner, W. (2008). "A simple model for describing hydraulic conductivity in unsaturated
726 porous media accounting for film and capillary flow." *Water Resources Research*, 44(11).
727 Philip, J. R., and De Vries, D. A. (1957). "Moisture movement in porous materials under temperature
728 gradients." *Eos, Transactions American Geophysical Union*, 38(2), 222-232.
729 Rahardjo, H., Santoso, V. A., Leong, E. C., Ng, Y. S., and Hua, C. J. (2012). "Performance of an
730 instrumented slope covered by a capillary barrier system." *Journal of geotechnical and geoenvironmental*
731 *engineering*, 138(4), 481-490.
732 Reinson, J. R., Fredlund, D. G., and Wilson, G. W. (2005). "Unsaturated flow in coarse porous media."
733 *Canadian geotechnical journal*, 42(1), 252-262.

734 Richards, B. G. (1965). “Measurement of the Free Energy of Soil Moisture by the Psychrometric
735 Technique Using Thermistors.” In: Aitchison, G.D. (Ed.), *Moisture Equilibria and Moisture Changes in*
736 *Soils Beneath Covered Areas*. A Symposium in Print. Butterworths &Co. Ltd., Sydney, Australia, pp. 35–46.
737 Rossi, C., and Nimmo, J. R. (1994). "Modeling of soil water retention from saturation to oven dryness."
738 *Water Resources Research*, 30(3), 701-708.
739 Scarfone, R., Lloret-Cabot, M., and Wheeler, S. J. (2018). "Numerical modelling of water breakthrough
740 in coarse soils initially at very low degree of saturation." In *Proc. of the 7th International Conference on*
741 *Unsaturated Soils*, Hong Kong, China, 3-5 Aug 2018.
742 Schubert, H., Herrmann, W., and Rumpf, H. (1975). "Deformation behaviour of agglomerates under
743 tensile stress." *Powder technology*, 11(2), 121-131.
744 Stormont, J. C., and Anderson, C. E. (1999). "Capillary barrier effect from underlying coarser soil layer."
745 *Journal of Geotechnical and Geoenvironmental Engineering*, 125(8), 641-648.
746 Stormont, J. C., and Morris, C. E. (1998). "Method to estimate water storage capacity of capillary
747 barriers." *Journal of Geotechnical and Geoenvironmental Engineering*, 124(4), 297-302.
748 Tami, D., Rahardjo, H., Leong, E. C., and Fredlund, D. G. (2004). "Design and laboratory verification of
749 a physical model of sloping capillary barrier." *Canadian Geotechnical Journal*, 41(5), 814-830.
750 Tokunaga, T. K. (2009). "Hydraulic properties of adsorbed water films in unsaturated porous media."
751 *Water resources research*, 45(6).
752 Tuller, M., and Or, D. (2001). "Hydraulic conductivity of variably saturated porous media: Film and
753 corner flow in angular pore space." *Water Resources Research*, 37(5), 1257-1276.
754 van Genuchten, M. T. (1980). "A closed-form equation for predicting the hydraulic conductivity of
755 unsaturated soils." *Soil science society of America journal*, 44(5), 892-898.
756 Vanapalli, S. K., Fredlund, D. G., and Pufahl, D. E. (1999). “The Influence of Soil Structure and Stress
757 History on the Soil–Water Characteristics of a Compacted Till.” *Géotechnique* 49 (2), 143–159.
758 Vanapalli, S. K., Sillers, W. S., and Fredlund, M. D. (1998). “The Meaning and Relevance of Residual
759 State to Unsaturated Soils.” In *Proceedings of the 51st Canadian Geotechnical Conference*, 1,101–108.
760 Edmonton, Alberta.

761 Wheeler, S. J., and Karube, D. (1996). “Constitutive Modelling.” In *Proceedings of the 1st International*
762 *Conference on Unsaturated Soils, Paris, France, 6-8 September 1995*, 3, 1123–1356. A.A. Belkema,
763 Rotterdam, the Netherlands.
764 Yang, H., Rahardjo, H., and Leong, E. C. (2006). "Behavior of unsaturated layered soil columns during
765 infiltration." *Journal of Hydrologic Engineering*, 11(4), 329-337.
766 Yang, H., Rahardjo, H., Leong, E. C., and Fredlund, D. G. (2004). "A study of infiltration on three sand
767 capillary barriers." *Canadian Geotechnical Journal*, 41(4), 629-643.
768 Zhan, T. L., and Ng, C. W. (2004). "Analytical analysis of rainfall infiltration mechanism in unsaturated
769 soils." *International Journal of Geomechanics*, 4(4), 273-284.
770 Zhang, Z. F. (2011). "Soil water retention and relative permeability for conditions from oven-dry to full
771 saturation." *Vadose Zone Journal*, 10(4), 1299-1308.
772
773

List of tables

Table 1. General properties of soils 1-11

Soil n°	Soil type	Reference*	k_s [m/s]	ϕ	D_{10} [mm]	D_{50} [mm]
1	Sand	N (4660)	$7.240x10^{-5}$	0.46	0.0647	0.3013
2	Sand	N (4661)	$1.320x10^{-4}$	0.43	0.0722	0.3113
3	Sand	N (4650)	$6.791x10^{-5}$	0.38	0.0722	0.3195
4	Loamy sand	N (4011)	$2.176x10^{-6}$	0.419	0.0174	0.1121
5	Loamy sand	N (4062)	$1.508x10^{-6}$	0.32	0.0265	0.1041
6	Shonai Sand	Me	$1.093x10^{-4}$	0.43	0.1317	0.3099
7	Sandy Loam	N (4172)	$3.738x10^{-6}$	0.42	-	0.0915
8	Silt Loam	N (4182)	$7.014x10^{-6}$	0.435	-	0.0296
9	Gilat Loam	Mu	$2.000x10^{-6}$	0.44	-	-
10	Rehovot Sand	Mu	$1.330x10^{-4}$	0.40	-	-
11	Grenoble 3 Sand	N (4442)	$5.000x10^{-5}$	0.385	0.1409	0.2859

* N (ID code): Nemes *et al*. (2001); Me: Mehta *et al*. (1994); Mu: Mualem (1976a).

Table 2. Fitted values of C^{Film} and X_D for soils 1-10

Soil n°	C^{Film} [m s^{-1}.$kPa^{1.5}$]	X_D (D_{10}) [mm.m s^{-1}.$kPa^{1.5}$]	X_D (D_{50}) [mm.m s^{-1}.$kPa^{1.5}$]
1	$6.842x10^{-8}$	$8.20x10^{-9}$	$3.82x10^{-8}$
2	$4.0919x10^{-8}$	$5.18x10^{-9}$	$2.23x10^{-8}$
3	$3.0120x10^{-8}$	$3.51x10^{-9}$	$1.55x10^{-8}$
4	$3.9372x10^{-8}$	$1.18x10^{-9}$	$7.60x10^{-9}$
5	$3.8297x10^{-8}$	$1.49x10^{-9}$	$5.86x10^{-9}$
6	$2.7805x10^{-9}$	$6.42x10^{-10}$	$1.51x10^{-9}$
7	$1.6153x10^{-7}$	-	$2.55x10^{-8}$
8	$1.5310x10^{-7}$	-	$8.02x10^{-9}$
9	$3.3616x10^{-8}$	-	-
10	$7.3879x10^{-10}$	-	-
Default	-	$2.35x10^{-9}$	$1.08x10^{-8}$

Table 3. Model parameter values for soils 1-11

Soil n°	n (VG)	α (VG) [kPa^{-1}]	S_{lr} (VG)	n (modVG)	α (modVG)	ξ (modVG)	s_{BWD} (modM) [kPa]
1	1.4153	2.2105	0.0864	1.4643	2.3245	0.0125	50
2	1.7129	1.3388	0.0780	1.7820	1.3553	0.0096	12
3	2.198	0.4434	0.0810	2.4487	0.4398	0.0108	40
4	1.6767	0.2348	0.1314	1.8519	0.2371	0.0204	40
5	1.3739	0.2826	0.0000	1.3739	0.2826	0.0000	400
6	3.9820	0.4598	0.0762	4.6368	0.4641	0.0105	4.7
7	1.2844	0.2253	0.0000	1.2844	0.2253	0.0000	200
8	1.2664	0.2286	0.0000	1.2664	0.2287	0.0000	600
9	2.4417	0.1709	0.1919	3.3255	0.1774	0.0287	14
10	3.1295	0.4645	0.0289	3.2450	0.4664	0.0038	8
11	6.3045	0.2244	0.2691	6.4199	0.2259	0.0232	6.475

Table 4. Material parameter values for the numerical analyses

Material	ϕ	k_s [m/s]	D_{10} [mm]	α [kPa^{-1}]	n	S_{lr} (VG)	ξ (modVG)	S_{ls}	s_{BWC} [kPa]	X_D [mm.m s^{-1}.$kPa^{1.5}$]
F.L. VG-M	0.38	$3x10^{-6}$	-	0.306	2.02	0.184	-	1	-	-
C.L. VG-M	0.30	10^{-2}	-	5.851	2.44	0.033	-	1	-	-
C.L. modVG-modM	0.30	10^{-2}	-	5.851	2.44	-	0.088	1	0.7	-
C.L. modVG-modM+LF	0.30	10^{-2}	5	5.851	2.44	-	0.088	1	0.7	$2.35x10^{-9}$

List of figures

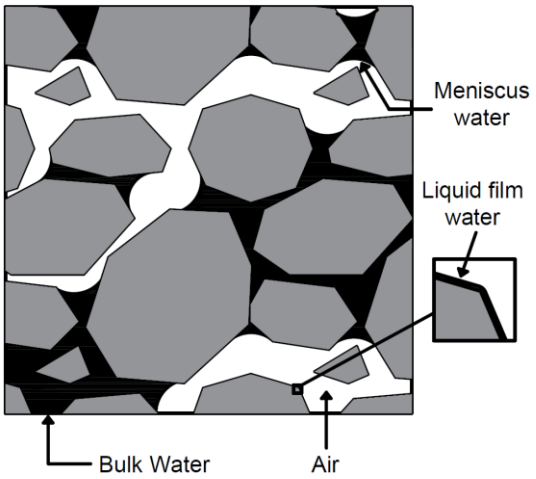

Fig. 1. Liquid water forms in unsaturated soils.

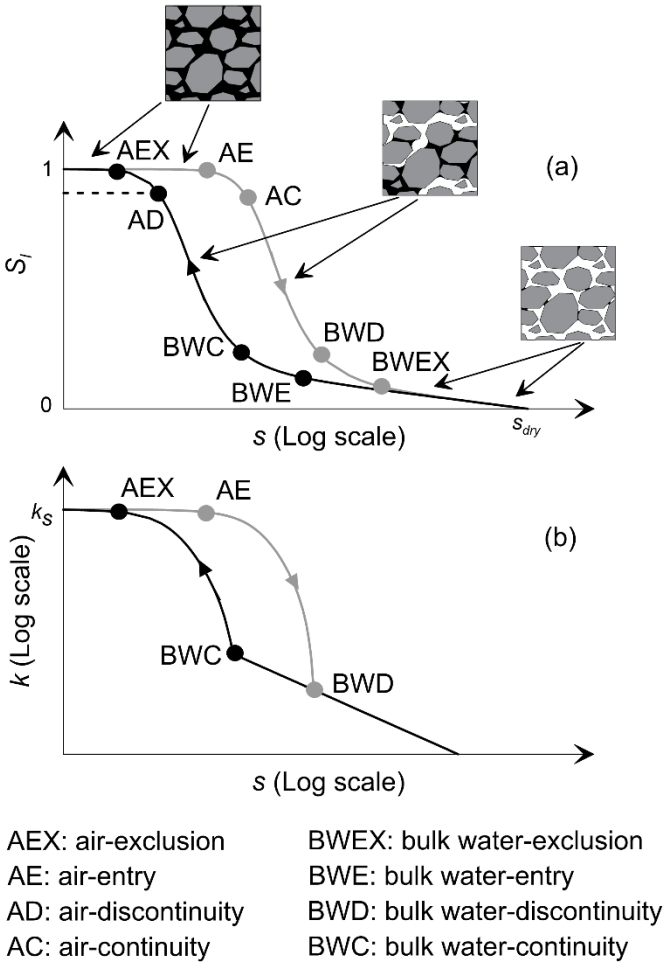

AEX: air-exclusion
AE: air-entry
AD: air-discontinuity
AC: air-continuity
BWEX: bulk water-exclusion
BWE: bulk water-entry
BWD: bulk water-discontinuity
BWC: bulk water-continuity

Fig. 2. Typical (a) SWRC and (b) SHCC, with key transition points indicated.

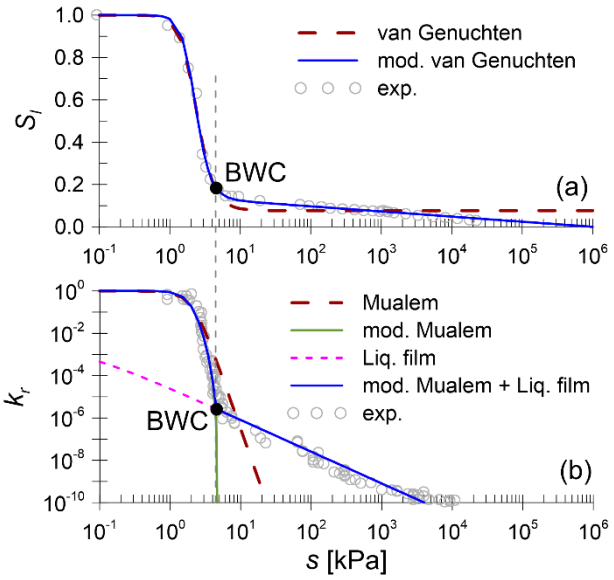

788

789 **Fig. 3.** Comparison between the hydraulic constitutive models and experimental data for Shonai sand (Mehta *et al.*

790 1994): (a) SWRC and (b) SHCC.

791

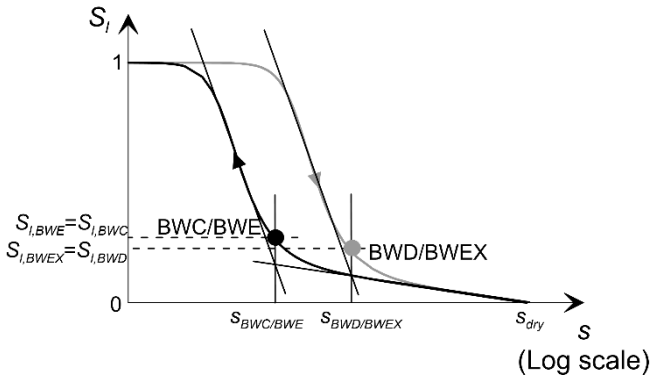

792

793 **Fig. 4.** Graphical procedure for simplified estimation of $S_{l,BWD}$, $S_{l,BWC}$, $S_{l,BWEX}$ and $S_{l,BWE}$.

794

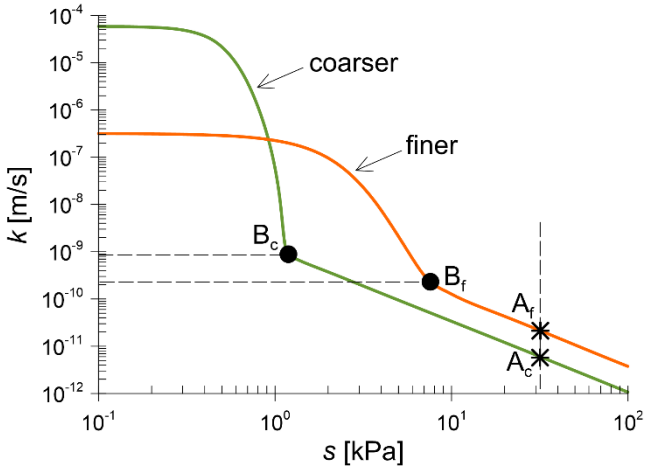

795

796 **Fig. 5.** Qualitative comparison between predicted SHCCs for a finer-grained soil and a coarser-grained.

797

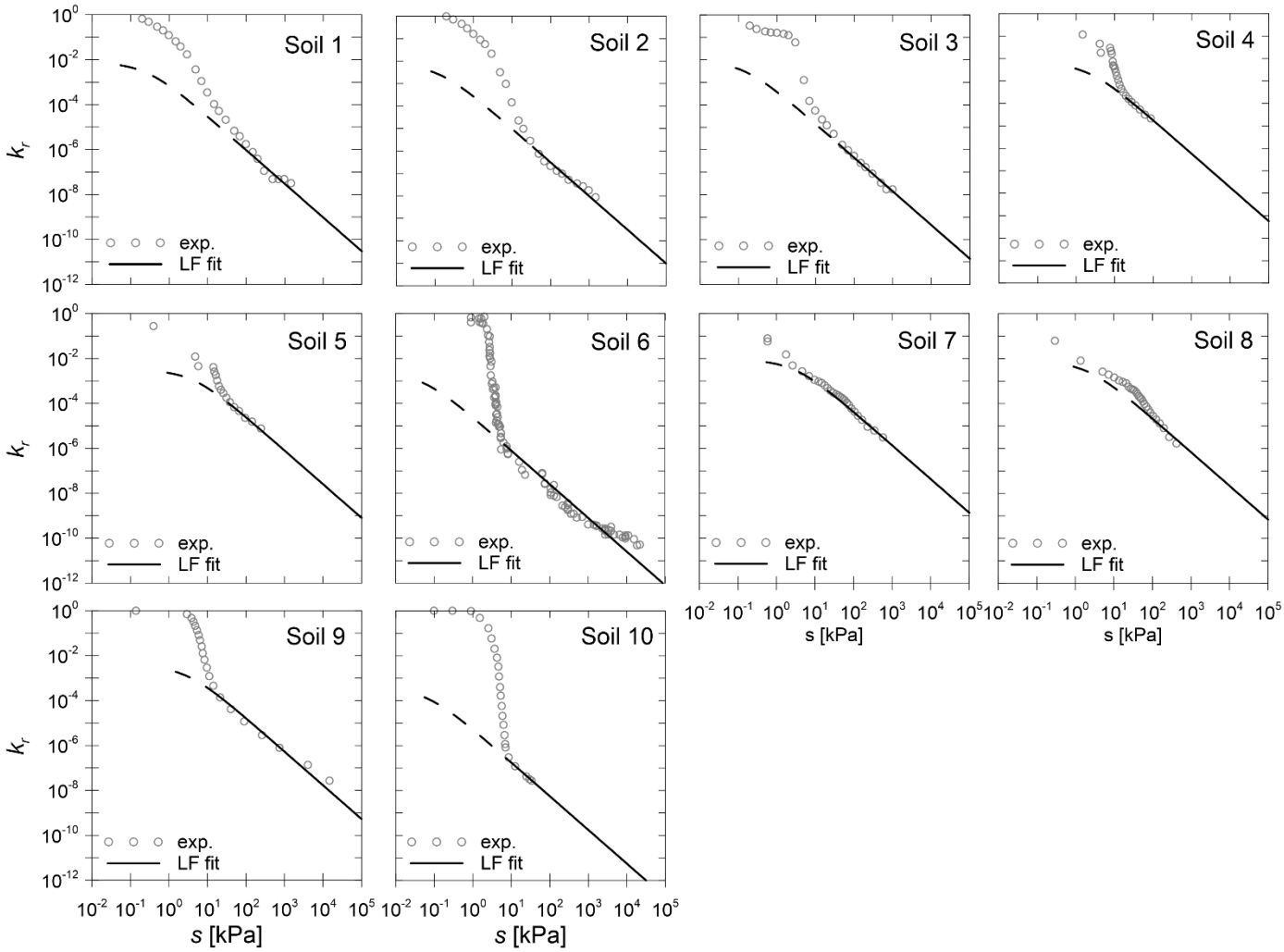

Fig. 6. Liquid film component of the hydraulic conductivity (Eq. 10) fitted to experimental data in the range where the hydraulic conductivity is governed by the liquid film component (soils 1-10).

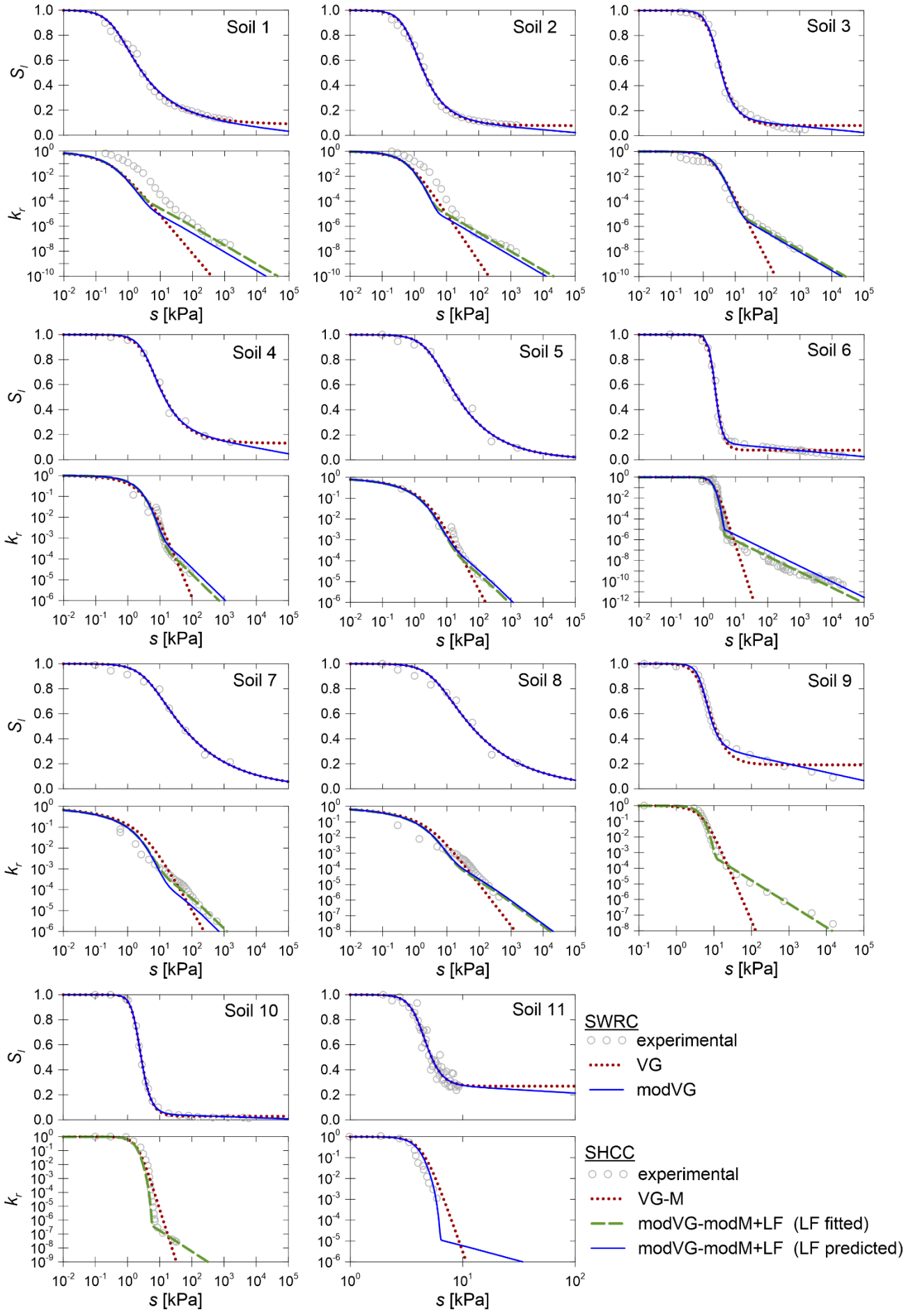

Fig. 7. Comparison between experimental data and SWRC and SHCC models for soils 1-11.

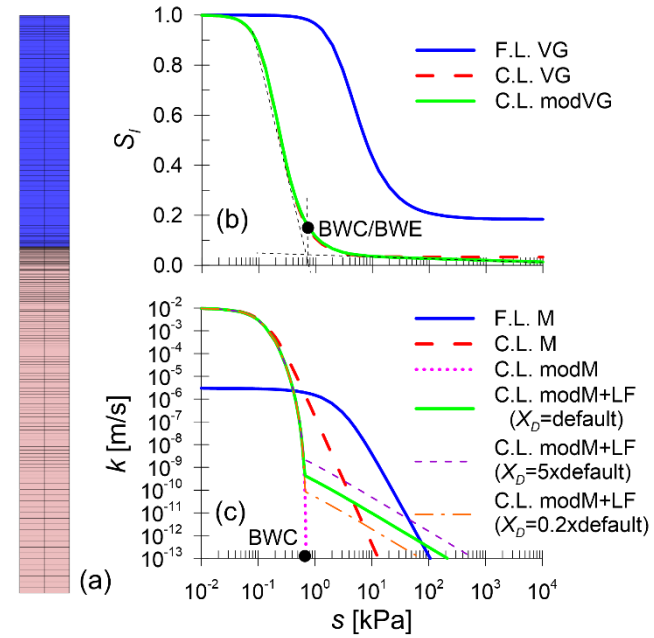

805

806 **Fig. 8.** Numerical model: (a) mesh and hydraulic properties of the materials, (b) SWRCs and (c) SHCCs.

807

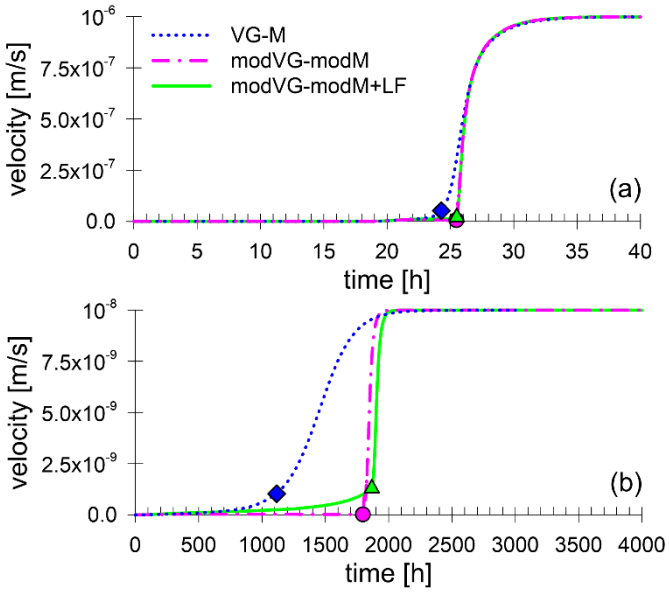

808

809 **Fig. 9.** Predicted time histories of water velocity across the interface for (a) infiltration rate i_1 and (b) infiltration rate i_2;
810 symbols indicate the times at breakthrough.

811

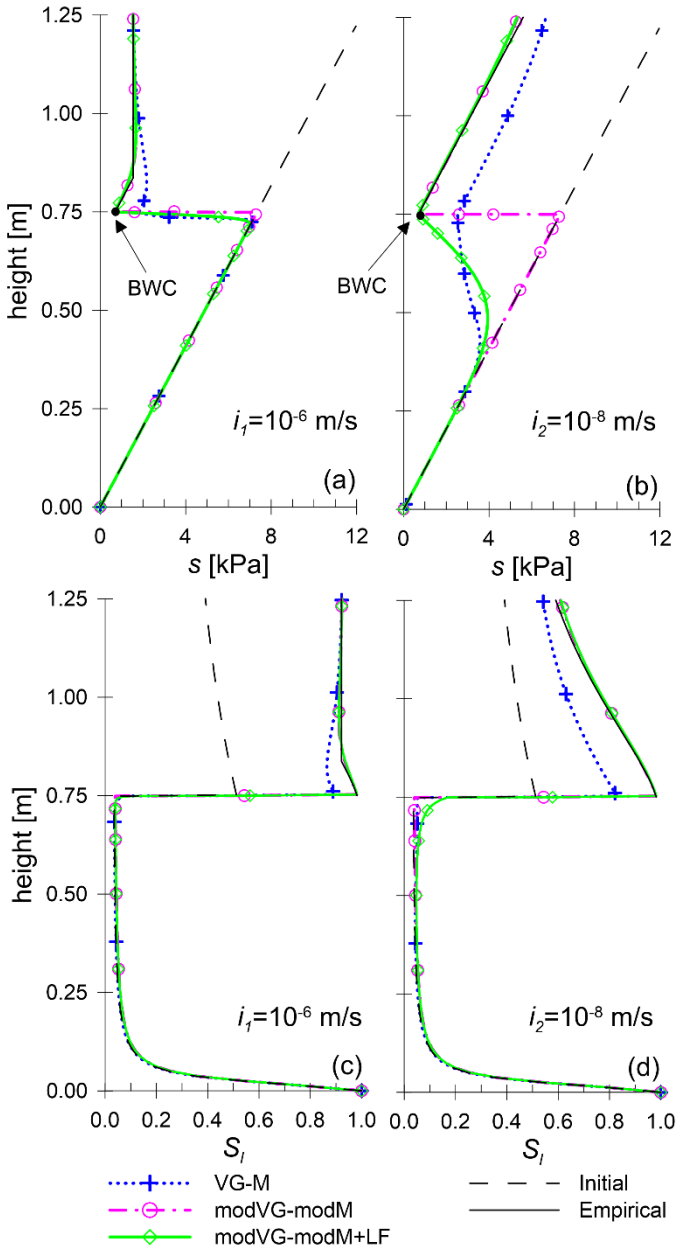

812

813 **Fig. 10.** Suction (a, b) and degree of saturation (c, d) profiles at breakthrough for infiltration rates i_1 and i_2.